A trajectory-based understanding of quantum interference

2008 J. Phys. A: Math. Theor. 41 435303

(http://iopscience.iop.org/1751-8121/41/43/435303)

IOP PUBLISHING JOURNAL OF PHYSICS A: MATHEMATICAL AND THEORETICAL

J. Phys. A: Math. Theor. **41** (2008) 435303 (23pp) doi:10.1088/1751-8113/41/43/435303

A trajectory-based understanding of quantum interference

A S Sanz and S Miret-Artés

Instituto de Física Fundamental, Consejo Superior de Investigaciones Científicas, Serrano 123, 28006 Madrid, Spain

E-mail: asanz@imaff.cfmac.csic.es and s.miret@imaff.cfmac.csic.es

Received 12 June 2008, in final form 8 August 2008
Published 30 September 2008
Online at stacks.iop.org/JPhysA/41/435303

Abstract

Interference is one of the most fundamental features which characterizes quantum systems. Here we provide an exhaustive analysis of the interfere dynamics associated with wave-packet superpositions from both the standard quantum-mechanical perspective and the Bohmian one. From this analysis, clear and insightful pictures of the physics involved in these kind of processes are obtained, which are of general validity (i.e., regardless of the type of wave packets considered) in the understanding of more complex cases where interference is crucial (e.g., scattering problems, slit diffraction, quantum control scenarios or, even, multipartite interactions). In particular, we show how problems involving wave-packet interference can be mapped onto problems of wave packets scattered off potential barriers.

PACS numbers: 03.65.−w, 03.65.Ta, 03.75.−b, 42.25.Hz

(Some figures in this article are in colour only in the electronic version)

1. Introduction

Over the last 15 years or so, fields such as the quantum information theory [1, 2], quantum computation [1, 2] and quantum control [3] have undergone a fast development. Simultaneously, due to the relevant role that *entanglement* plays in all these fields, the idea of this phenomenon being the most distinctive feature of quantum mechanics has also grown in importance, although this is already infered from earlier works [4]. However, despite this relevance, in our opinion *quantum interference* (together with diffraction) can still be considered of more fundamental importance within the quantum theory, its most striking manifestation being, most surely, the two-slit experiment, which 'has in it the heart of quantum mechanics. In reality, it contains the *only* mystery [...], quoting Feynman [5]. Quantum interference is the direct, observable consequence of the *coherent* superposition

of (quantum) probability fields. This is precisely what is special about it: interferences in quantum mechanics are not associated with or produced by a sudden transfer of energy (in the way of a perturbation) along a material medium, as happens with classical waves. It is worth stressing that, apart from its importance at a conceptual and fundamental level, quantum interference is also involved in a very wide range of experimental situations and applications. SQUIDs or superconducting quantum interference devices [6], the coherent control of chemical reactions [3], atom and molecular interferometry [7] (in particular, with BECs [8–10], where different techniques to recombine the split beams are used [11–14]) or Talbot/Talbot-Lau interferometry with relatively heavy particles (e.g., Na atoms [15] and BECs [16]) are just some examples. Moreover, it is also important to note the role played by interference when dealing with multipartite entangled systems as an indicator of the loss of coherence induced by the interaction between the different subsystems, for instance.

The actual understanding and interpretation of interference phenomena arises from the, somehow, physical 'reality' ascribed to the superposition principle. According to this (mathematical) principle, wave fields can be decomposed and then recombined again to produce and explain the interference patterns observed. However, in nature, wave fields constitute a whole and, therefore, it is important to determine what this behavior means when we are dealing with quantum phenomena displaying interference. Here we analyze such consequences in the case of coherent superpositions of Gaussian wave packets by means of properties which can be derived from standard quantum mechanics (but that, to our knowledge, are not considered at all in the literature) and also from Bohmian mechanics [17, 18]. In the latter case, we will show that there exists a sort of mapping which allows us to translate wave-packet interference problems onto problems of single wave packets scattered off by potential barriers. The interest in this kind of superpositions arises from the fact that, rather than simple academical examples whose interference dynamics is well known in the literature [19, 20], such superpositions are experimentally realizable (and, indeed, used) in atom interferometry [11–14]. In figure 1, for instance, we have sketched two types of experiments where coherent superpositions of Gaussian wave packets can be produced. Moreover, it is also important to highlight the interest that the analysis presented here can have to better understand scattering processes, quantum control scenarios or many-particle interactions, where interference plays a fundamental role, as well as to design, develop, improve and/or implement new trajectory-based algorithms [21], where one of the main drawbacks is the presence of nodes in the wavefunction produced by interferences.

The organization of this paper is as follows. To be self-contained, in section 2 we provide a brief overview of quantum interference and Bohmian mechanics, as well as some interesting properties which will be used and further discussed in following section. In section 3, we present the analysis of wave-packet superposition dynamics and the main results derived from it. Thus, we begin with a brief overview on (single) wave-packet dynamics and its properties, and then we introduce our non-standard analysis of two wave-packet interference processes and the analogy of this problem with wave-packet scattering off barriers. Finally, in section 4, we provide a summary of the main conclusions in this work as well as a discussion on their interest in more complex problems.

2. Interference and quantum trajectories

Since the Schrödinger equation is linear, it satisfies the superposition principle. Thus, given ψ_1 and ψ_2 satisfying separately this equation, its superposition,

$$\Psi(\mathbf{r}, t) = \psi_1(\mathbf{r}, t) + \psi_2(\mathbf{r}, t), \tag{1}$$

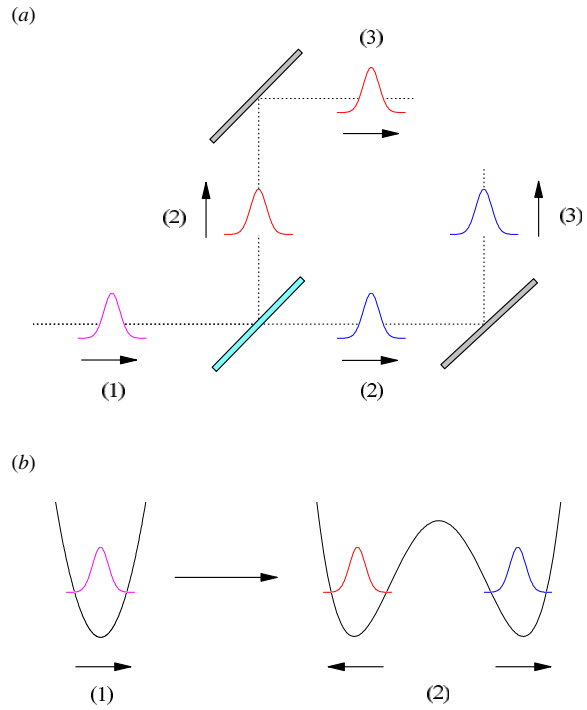

Figure 1. Two situations which give rise to a description of the wavefunction as a superposition of two wave packets at a certain time. (*a*) After reaching a beam splitter, an incoming wave packet (1) splits into two ones (2). These wave packets move apart until they reach two reflectant mirrors, which redirect their propagation (3). The wavefunction describing the evolution of these two wave packets is a superposition which will display interference when they 'collide' after some time in future (this fourth step has not been represented). (*b*) A wave packet confined in a potential well (1) is split into two wave packets by creating a barrier inside the potential (2) and then pulling outward the two new potential wells (each containing a new wave packet). If the potential is turned off and the wave packets pulled inward, the (superposition) wavefunction that describes them will again display interference (again, as in the previous case, we have not represented this step), as can be seen in BEC interferometric experiments.

will also be a valid solution. Now, the wave amplitude Ψ is not an *observable* magnitude, but the probability density, $\rho = |\Psi|^2$, which provides a statistical description of the system [22]. Due to the connection between Ψ and ρ, it is clear that the superposition principle does not hold for the latter. Note that, after expressing ψ_i $(i = 1, 2)$ in polar form, i.e., $\psi_i = \rho_i^{1/2}\, \mathrm{e}^{\mathrm{i}S_i/\hbar}$, we find

$$\rho = \rho_1 + \rho_2 + 2\sqrt{\rho_1\rho_2}\cos\varphi, \tag{2}$$

where $\varphi = (S_2 - S_1)/\hbar$. The interference term in equation (2) connects *coherently* the probability densities (ρ_1 and ρ_2) related to each partial wave (ψ_1 and ψ_2, respectively).

Since ρ describes the statistical distribution associated with a particle ensemble regardless of whether there is an interaction potential connecting them or not, one can define an associate probability current density as

$$\mathbf{J} = \frac{1}{m}\,\mathrm{Re}[\Psi^*\hat{\mathbf{p}}\Psi] = -\frac{\mathrm{i}\hbar}{2m}[\Psi^*\nabla\Psi - \Psi\nabla\Psi^*], \tag{3}$$

which indicates the flow of such an ensemble, with $\hat{\mathbf{p}} = -\mathrm{i}\hbar\nabla$ being the momentum (vector) operator. Substituting (1) into (3), with the ψ_i expressed in polar form, yields

$$\mathbf{J} = \frac{1}{m}\left[\rho_1\nabla S_1 + \rho_2\nabla S_2 + \sqrt{\rho_1\rho_2}\nabla(S_1+S_2)\cos\varphi + \hbar\left(\rho_1^{1/2}\nabla\rho_2^{1/2} - \rho_2^{1/2}\nabla\rho_1^{1/2}\right)\sin\varphi\right], \tag{4}$$

which clearly shows that the superposition principle does not hold either for $\mathbf{J}$. The two magnitudes ρ and $\mathbf{J}$ are related through the continuity equation,

$$\frac{\partial\rho}{\partial t} + \nabla\mathbf{J} = 0, \tag{5}$$

which can be easily derived from the Schrödinger equation after multiplying both sides by Ψ^*, adding to the resulting equation its complex conjugate, and then rearranging terms.

Within this hydrodynamical picture of quantum mechanics [23], one can always further proceed as in classical mechanics and determine the probability streamlines, i.e., the lines along which the probability flows. Consider the same polar ansatz used above, but for the total wavefunction, $\Psi = \rho^{1/2}\,\mathrm{e}^{\mathrm{i}S/\hbar}$. After substituting it into the Schrödinger equation and rearranging terms, one obtains

$$\frac{\partial S}{\partial t} + \frac{(\nabla S)^2}{2m} + V + Q = 0 \tag{6}$$

$$\frac{\partial\rho}{\partial t} + \frac{1}{m}\nabla(\rho\nabla S) = 0 \tag{7}$$

from the real and imaginary parts of the resulting expression, respectively. Equation (7) is the continuity equation (5), with $\mathbf{J} = (\rho\nabla S)/m$. Equation (6), more interesting from a dynamical viewpoint, is the quantum Hamilton–Jacobi equation, which allows us to reinterpret the whole quantum-mechanical formalism in terms of the eventual paths that the system can pursue when it is considered as a particle. These paths are defined as solutions of the equation of motion

$$\dot{\mathbf{r}} = \frac{\nabla S}{m} = \frac{\mathbf{J}}{\rho} = -\frac{\mathrm{i}\hbar}{2m}\frac{\Psi^*\nabla\Psi - \Psi\nabla\Psi^*}{\Psi^*\Psi}, \tag{8}$$

where S represents a quantum generalized action. Note that considering equation (8) means introducing a new conceptual element into quantum mechanics: well-defined trajectories in both space and time. This new element constitutes the essence of what is known nowadays as Bohmian mechanics [17, 18], a quantum mechanics based on the hydrodynamical equations (6) and (7) plus the particle equation of motion (8). Because of the relationship between particles and waves in Bohmian mechanics, the initial momentum of particles is predetermined by $\Psi(\mathbf{r}, 0)$ and therefore it is not necessary to enquire about its value. Only initial positions are freely, randomly chosen, with the constraint that their distribution is given by $\rho(\mathbf{r}, 0)$.

As infered from equation (6), the difference with respect to classical mechanics is that quantum trajectories evolve under the action of both the external potential V and the so-called quantum potential,

$$Q = -\frac{\hbar^2}{2m}\frac{\nabla^2\rho^{1/2}}{\rho^{1/2}}, \tag{9}$$

which introduces into the quantum motion the context dependence and nonlocality necessary for the particles (distributed initially according to $\rho(\mathbf{r}, 0)$) to reproduce the patterns of standard quantum mechanics when they are considered in a large statistical number. The quantum dynamics is thus ruled by a total effective potential $V_{\mathrm{eff}}(\mathbf{r}, t) = V(\mathbf{r}) + Q(\mathbf{r}, t)$. An interesting property of the quantum potential can be found when one computes the energy expected value,

$$\bar{E} = \langle\hat{H}\rangle = \langle\hat{T}\rangle + \langle\hat{V}\rangle, \tag{10}$$

which, in Bohmian mechanics, just consists of determining the ensemble average energy. The first term in (10) is the expected value of the kinetic energy, with $\hat{T} = -(\hbar^2/2m)\nabla^2$ denoting the kinetic operator. When the polar ansatz of the wavefunction is considered, we obtain

$$\langle \hat{T} \rangle = -\frac{\hbar^2}{2m} \int R \left[\nabla^2 R - \frac{R}{\hbar^2} (\nabla S)^2 \right] \mathrm{d}\mathbf{r} + \frac{\hbar}{2im} \int \nabla(\rho \nabla S)\, \mathrm{d}\mathbf{r}. \tag{11}$$

From (7), we have

$$\int \nabla \mathbf{J}\, \mathrm{d}\mathbf{r} = -\int \frac{\partial \rho}{\partial t}\, \mathrm{d}\mathbf{r} = -\frac{\partial}{\partial t} \int \rho\, \mathrm{d}\mathbf{r} = 0, \tag{12}$$

since the probability density conserves in the whole space. In other words, if the system is closed, no probability can flow to or from the region where this system is defined; this is the probabilistic analog of the energy conservation principle. Therefore, (11) and (10) become

$$\langle \hat{T} \rangle = \int \left(-\frac{\hbar^2}{2m} \frac{\nabla^2 R}{R} \right) \rho\, \mathrm{d}\mathbf{r} + \int \frac{(\nabla S)^2}{2m} \rho\, \mathrm{d}\mathbf{r} = \langle Q \rangle + \frac{\langle p^2 \rangle}{2m} \tag{13}$$

and

$$\bar{E} = \bar{E}_k + \bar{Q} + \bar{V} = \bar{E}_k + \bar{V}_{\mathrm{eff}}, \tag{14}$$

respectively, where $\bar{E}_k$ is the average (expected value) contribution from the kinetic energy associated with each particle from the ensemble. Thus, note that, although Q is usually assigned the role of a quantum potential energy, since it is obtained from the kinetic operator and contributes to the expected value of the kinetic energy, one can also consider it as a quantum kinetic energy. More importantly, putting aside such considerations, Q is the only responsible for making quantum dynamics so different from classical ones due to its nonlocal nature ($\bar{E}_k$ and $\bar{V}$ only contain local information)—note that Q contains information about the whole quantum state and therefore supplies it to the particle at the particular point where it is located. From a practical or computational point of view, this explains why a good representation of the momentum operator has to contain a wide spectrum of momenta. Furthermore, (14) also indicates that classical-like behaviors appear whenever the part of the energy associated with the quantum potential becomes sufficiently small.

To conclude this section, we are going to discuss another interesting property of quantum motion: in Bohmian mechanics two trajectories cannot cross the same point at the same time in the configuration space (note that, in classical mechanics, this only happens in the phase space). In order to prove this, consider that two velocities are assigned to the same point $\mathbf{r}$, $v_1(\mathbf{r})$ and $v_2(\mathbf{r})$, with $v_1 \neq v_2$. From (8) we know that these velocities are directly related to some wavefunctions $\psi_1(\mathbf{r})$ and $\psi_2(\mathbf{r})$, respectively. If both wavefunctions are solutions of the same Schrödinger equation, the only possibility for them to be different at the same space point x is that their phases differ, as much, in a time-dependent function (and/or space-independent constant), i.e.,

$$S_2(\mathbf{r}, t) = S_1(\mathbf{r}, t) + \phi(t). \tag{15}$$

Now, since the velocities are the gradient of these functions, it is clear that v_2 has to be equal to v_1 necessary if the wavefunction does not vanish at $\mathbf{r}$.

3. Simple examples of quantum interference with Gaussian wave packets

3.1. The free Gaussian wave packet

For the sake of simplicity, we are going to consider one-dimensional Gaussian wave packets, although the results presented in this work can be generalized to more dimensions and other

types of wave packets straightforwardly. The evolution of a free Gaussian wave packet can be described by

$$\Psi(x,t) = A_t\, \mathrm{e}^{-(x-x_t)^2/4\tilde{\sigma}_t\sigma_0 + \mathrm{i}p(x-x_t)/\hbar + \mathrm{i}Et/\hbar}, \tag{16}$$

where $A_t = \left(2\pi\tilde{\sigma}_t^2\right)^{-1/4}$ and the complex time-dependent spreading is

$$\tilde{\sigma}_t = \sigma_0\left(1 + \frac{\mathrm{i}\hbar t}{2m\sigma_0^2}\right). \tag{17}$$

From (17), the spreading of this wave packet at time t is

$$\sigma_t = |\tilde{\sigma}_t| = \sigma_0\sqrt{1 + \left(\frac{\hbar t}{2m\sigma_0^2}\right)^2}. \tag{18}$$

Due to the free motion, $x_t = x_0 + v_p t$ ($v_p = p/m$ is the propagation velocity) and $E = p^2/2m$, i.e., the centroid of the wave packet moves along a classical rectilinear trajectory. This does not mean, however, that the expected (or average) value of the wave-packet energy is equal to E, which, according to equation (14), results

$$\bar{E} = \frac{p^2}{2m} + \frac{\hbar^2}{8m\sigma_0^2}. \tag{19}$$

In (19) we thus observe two contributions. The first one is associated with the propagation or translation of the wave packet, while the latter is related to its spreading and has, therefore, a purely quantum-mechanical origin. From now on, we will denote them as E_p and E_s, respectively, noting that none of them depends on time. Expressing E_s in terms of an *effective* momentum p_s (i.e., $E_s = p_s^2/2m$), we find

$$p_s = \frac{\hbar}{2\sigma_0}, \tag{20}$$

which resembles Heisenberg's uncertainty relation. Note that, in the case of *non-dispersive* Airy wave packets [24], we will find $p_s = 0$.

With the previous definition, the wave packet dynamics can be referred to two well-defined velocities: v_p and v_s, whose relationship is shown to play an important role in the type of effects that one can observe when dealing with wave packet superpositions. To better understand this statement, consider equation (18). Defining the timescale

$$\tau = 2m\sigma_0^2/\hbar, \tag{21}$$

we find that, if $t \ll \tau$, the width of the wave packet remains basically constant with time, $\sigma_t \approx \sigma_0$ (i.e., for practical purposes, it is roughly time independent up to time t). In contrast, if $t \gg \tau$, the width of the wave packet increases linearly with time ($\sigma_t \approx \hbar t/2m\sigma_0$). Of course, in between there is a smooth transition; from (18) it is shown that the progressive increase of σ_t describes a hyperbola when this magnitude is plotted versus time. These are 'dynamical' relationships in the sense that the dynamical behavior of the wave packet is known comparing the actual time t with the effective time τ. When we are dealing with general wave packets, *a priori* we do not have an effective time τ to compare with. This inconvenience can be avoided if we consider the interpretive framework provided by v_p and v_s, which can be estimated from the initial state through equation (13). Within this framework, we can find a way to know which process—spreading or translational motion—is going to determine the wave packet dynamics, as follows. Expression (18) can be rewritten in terms of v_s as

$$\sigma_t = |\tilde{\sigma}_t| = \sigma_0\sqrt{1 + \left(\frac{v_s t}{\sigma_0}\right)^2}. \tag{22}$$

Now, consider that t is the time that takes the wave-packet centroid to cover a distance $d = v_p t \approx \sigma_0$. Introducing this result into (22), we obtain

$$\sigma_t = |\tilde{\sigma}_t| = \sigma_0 \sqrt{1 + \left(\frac{v_s}{v_p}\right)^2}. \tag{23}$$

This time-independent expression shows that, only using information about the initial preparation of the wave packet, we can obtain information on its subsequent dynamical behavior. Thus, $t \ll \tau$ is equivalent to having an initial wave packet prepared with $v_s \ll v_p$: the translational motion will be much faster than the spreading of the wave packet. On the other hand, $t \gg \tau$ is equivalent to $v_s \gg v_p$: the wave packet spreads very rapidly in comparison with its advance along x. A nice illustration of the 'competition' between v_p and v_s can be found in [25], where (for $|x_0| \approx \sigma_0$) it is shown that: (1) if v_p is dominant, the asymptotic motion is basically a classical-like motion (no spreading in comparison with the distances covered by particles), while (2) if v_s is dominant, although the motion is classical like (i.e., there is an asymptotic constant velocity, v_s), it has a purely quantum-mechanical origin and therefore eventual effects produced within this regime will also be purely quantum mechanical.

3.2. Dynamics of coherent wave-packet superpositions

Depending on whether the interference is localized in time within a certain space region or it remains stationary after some time, we can distinguish two types of processes or experiments: collision like (e.g., BEC interferometry) and diffraction like (e.g., the double-slit experiment), respectively. These behaviors are associated with the ratio between v_p and v_s: collision-like experiments are characterized by $v_p \gg v_s$, while diffraction-like experiments by $v_p \ll v_s$. Now, consider a general coherent superposition

$$\Psi = c_1\psi_1 + c_2\psi_2, \tag{24}$$

where the partial waves ψ_i are normalized Gaussian wave packets, as in (16), which propagate with opposite velocities v_p and where the centers are initially far enough in order to minimize the overlapping, i.e., $\rho_1(\mathbf{r}, 0)\rho_2(\mathbf{r}, 0) \approx 0$. As shown below, both the v_p/v_s ratio and the weighting factors c_1 and c_2 are going to influence the topology of the quantum trajectories. Since the wave packets are well apart initially, we find that the weighting factors satisfy the relation $|c_1|^2 + |c_2|^2 = 1$, which allows us to re-express (24) more conveniently as

$$\Psi = c_1(\psi_1 + \sqrt{\alpha}\psi_2), \tag{25}$$

where $\alpha = (c_2/c_1)^2$. From (25), we find that the probability density and the quantum current density read as

$$\rho = c_1^2[\rho_1 + \alpha\rho_2 + 2\sqrt{\alpha}\sqrt{\rho_1\rho_2}\cos\varphi], \tag{26}$$

$$\mathbf{J} = \frac{c_1^2}{m}\Big[\rho_1\nabla S_1 + \alpha\rho_2\nabla S_2 + \sqrt{\alpha}\sqrt{\rho_1\rho_2}\nabla(S_1 + S_2)\cos\varphi + \hbar\sqrt{\alpha}\left(\rho_1^{1/2}\nabla\rho_2^{1/2} - \rho_2^{1/2}\nabla\rho_1^{1/2}\right)\sin\varphi\Big], \tag{27}$$

respectively. Also, dividing equation (27) by (26), as in (8), we can obtain the associate quantum trajectories from the equation of motion

$$\dot{\mathbf{r}} = \frac{1}{m}\frac{\rho_1\nabla S_1 + \alpha\rho_2\nabla S_2 + \sqrt{\alpha}\sqrt{\rho_1\rho_2}\nabla(S_1 + S_2)\cos\varphi}{\rho_1 + \alpha\rho_2 + 2\sqrt{\alpha}\sqrt{\rho_1\rho_2}\cos\varphi} + \sqrt{\alpha}\frac{\hbar}{m}\frac{\left(\rho_1^{1/2}\nabla\rho_2^{1/2} - \rho_2^{1/2}\nabla\rho_1^{1/2}\right)\sin\varphi}{\rho_1 + \alpha\rho_2 + 2\sqrt{\alpha}\sqrt{\rho_1\rho_2}\cos\varphi}. \tag{28}$$

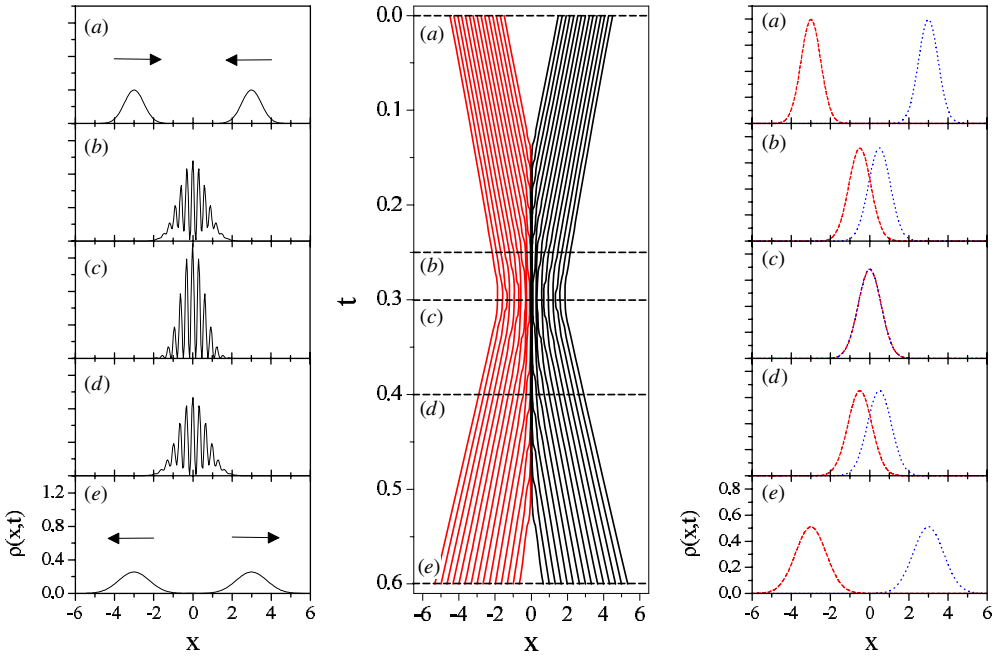

Figure 2. Left: from (*a*) to (*d*), snapshots illustrating the time evolution of two colliding Gaussian wave packets, with $v_p = 10$ and $v_s = 1$. Center: the same process as in the left column, by visualized in terms of quantum trajectories. The perpendicular dashed lines mark cuts in time corresponding with the same labels as in the figures of the left column. Right: interpretation of the process in the left column according to the quantum trajectories shown in the central column.

As can be noted, in this expression there are two well-defined contributions, which are related to the effects caused by the interchange of the wave packets (or the associate partial fluxes) on the particle motion (specifically, on the topology displayed by the corresponding quantum trajectories) after the interference process; note that the first contribution is even after interchanging only the modulus or only the phase of the wave packets, while the second one changes its sign with these operations. From the terms that appear in each contribution, it is apparent that the first contribution is associated with the evolution of each individual flux as well as with their combination. Thus, it provides information about both the asymptotic behavior of the quantum trajectories and also about the interference process (whenever the condition $\rho_1(\mathbf{r}, t)\rho_2(\mathbf{r}, t) \approx 0$ is not satisfied). On the other hand, the second contribution describes interference effects connected with the asymmetries or differences of the wave packets. For instance, their contribution is going to vanish if they are identical and coincide at $x = 0$ although their overlapping is nonzero.

Let us first consider the collision-like case. For the sake of simplicity and without loss of generality, we will assume $\alpha = 1$, with both wave packets being identical and propagating in opposite directions at the same speed. Also, for simplicity in the discussion, we will refer to the regions where ψ_1 and ψ_2 are initially placed as I and II, respectively. In standard quantum mechanics, a physical reality is assigned to the superposition principle, which in this case means that, after the wave packets have maximally interfered at $t_{\max}^{\text{int}}$ (panel (*c*) in the left column of figure 2), ψ_1 moves to region II and ψ_2 to region I. As mentioned above, the wave packets (or, more specifically, their associate probability densities) represent

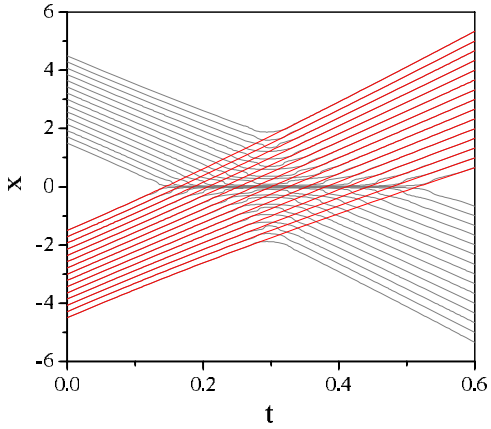

Figure 3. Bohmian trajectories associated with a Gaussian wave-packet superposition (gray) and a single Gaussian wave packet (red). As shown, the presence of the other wave packet makes the dynamics to avoid the crossing in the central part; the asymptotic part remains being the same as without presence of other wave packet. Here $v_p = 10$ and $v_s = 1$.

the statistical behavior of a swarm of identical, noninteracting quantum particles distributed accordingly. Therefore, within the standard view arising from the superposition principle, one would expect to observe crossings between trajectories in a certain time range around $t_{\max}^{\text{int}}$. However, this is not the behavior displayed by the Bohmian trajectories displayed in the central panel of figure 2, which avoid such crossings during the time range where interference effects are important. Note that quantum-mechanical statistics are characterized by keeping the coherence and transmitting it to the corresponding quantum dynamics, as infers from equation (28). Thus, the interference process has to be interpreted in a different way (than the standard quantum-mechanical one) when it is analyzed from a quantum trajectory perspective. As inferred from equation (28), for identical (but counter-propagating) wave packets, the velocity field vanishes along $x = 0$ at any time. This means that there cannot be any probability density (or particle) flux between regions I and II at any time. Therefore, trajectories starting in one of these regions will never cross to the other one and vice versa. Hence the final outgoing wave packets in panel (*e*) in the left column of figure 2 necessarily describe exactly the same swarms of particles associated with the wave packets that we had in their respective regions initially (see panel (*a*) of the same figure). The whole process can then be understood as a sort of bouncing motion of the wave packets once they have reached the intermediate position between them, as schematically represented in the right column of figure 2.

But, if the two swarms of trajectories do not cross each other, why does the swarm associated initially with one of the wave packets behave asymptotically as associated with the other one, as seen in figure 3? According to the standard description based on the superposition principle, the wave packets cross. This can be understood as a transfer or interchange of probabilities from region I to region II and vice versa. On the other hand, from a dynamical (quantum trajectory) viewpoint, this also means that the sign of the associate velocity field will change after the collision. That is, before the collision its sign points onward (toward $x = 0$) and after the collision it points outward (diverging from $x = 0$)—at $t_{\max}^{\text{int}}$ it does not point anywhere, but remains *steady*. Thus, like in a particle–particle elastic scattering process particles exchange their momenta, here the swarms of particles will exchange their probability distributions 'elastically'. This is nicely illustrated in figure 3: after the collision,

the two swarms of trajectories (gray lines) bounce backward and follow the paths that would be pursued by non-deflected particles (red lines). We can describe this process analytically as follows. Initially, depending on the region where the trajectories are launched from, they are described approximately by

$$\dot{\mathbf{r}}_{\mathrm{I}} \approx \nabla S_1/m \qquad \text{or} \qquad \dot{\mathbf{r}}_{\mathrm{II}} \approx \nabla S_2/m. \tag{29}$$

Now, asymptotically (for $t \gg t_{\max}^{\mathrm{int}}$), equation (28) can be expressed as

$$\dot{\mathbf{r}} \approx \frac{1}{m}\frac{\rho_1 \nabla S_1 + \rho_2 \nabla S_2}{\rho_1 + \rho_2}, \tag{30}$$

where we make use of the approximation $\rho_1(\mathbf{r}, t)\rho_2(\mathbf{r}, t) \approx 0$. Note that this approximation also means that the total probability density, $\rho = \rho_1 + \rho_2$, is nonzero only on the space regions covered by either ρ_1 or ρ_2. Specifically, in region I we will have $\rho \approx \rho_2$ and in region II, $\rho \approx \rho_1$. When this result is introduced into equation (30), we finally obtain

$$\dot{\mathbf{r}}_{\mathrm{I}} \approx \nabla S_2/m \qquad \text{and} \qquad \dot{\mathbf{r}}_{\mathrm{II}} \approx \nabla S_1/m, \tag{31}$$

which reproduce the dynamics observed asymptotically. This trajectory picture thus provides us with a totally different interpretation of wave-packet interference with respect to the standard one: although probability distributions transfer, particles remain always within the domains defined by their corresponding initial distributions (which have been here as regions I and II). The *non-crossing* property of Bohmian mechanics (see section 2) thus makes apparent the constraint that exists for the quantum probability flux, which goes beyond the separability of fluxes implicit in the superposition principle.

In the diffraction-like case, the spreading is faster than the propagation, this being the reason why we observe the well-known quantum trajectories of a typical two-slit experiment in the *Fraunhofer region* [19, 26]. It is relatively simple to show [20] that, in this case, the asymptotic solutions of equation (28) are

$$x(t) \approx 2\pi n \frac{\sigma_0}{x_0}\,(v_s t)\,, \tag{32}$$

with $n = 0, \pm 1, \pm 2, \ldots$. That is, there are bunches of quantum trajectories whose slopes are quantized quantities (through n) proportional to v_s. This means that, when equation (28) is integrated exactly, one will observe quantized bunches of trajectories which, on average, are distributed around the value given by equation (32).

3.3. Asymmetric coherent superpositions

In the previous subsection, we have studied interference processes with identical Gaussian wave packets propagating symmetrically with respect to $x = 0$. However, what happens in other more general situations where neither the wave packets are identical nor their weights? Although one could think of many different possibilities, it is enough to consider three cases in order to already obtain an insight on the related physics. The criterion followed to classify these cases is based on which property of the wave packets is varied (with respect to the symmetric case described in section 3.2) or considered at a time:

- Case A: Different modulus of the initial average momentum ($|p_{01}| \neq |p_{02}|$).
- Case B: Different initial spreading ($\sigma_{01} \neq \sigma_{02}$).
- Case C: Different weights ($c_1 \neq c_2$ or, equivalently, $\alpha \neq 1$).

Since the collision-like case is simpler to understand than the diffraction-like one, below we will assume $v_p \gg v_s$, although generalizing to any v_p/v_s ratio is straightforward.

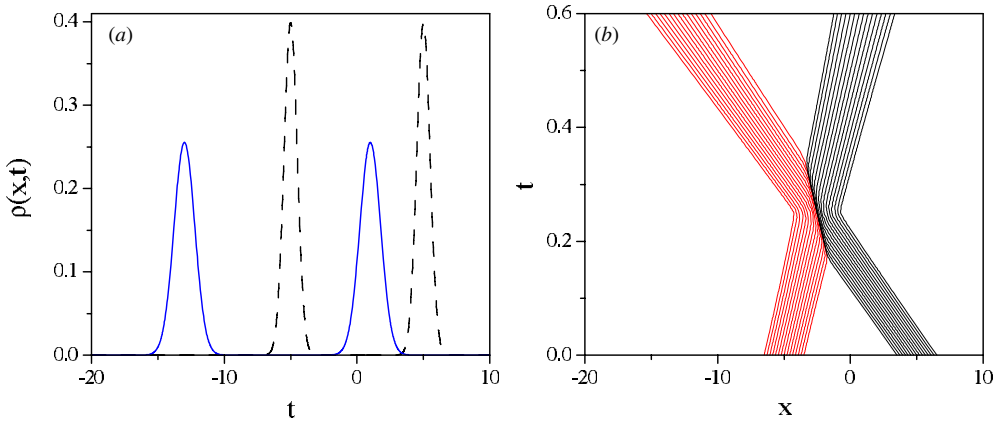

Figure 4. (*a*) Probability density at $t = 0$ (black dashed line) and $t = 0.6$ (blue solid line) for a wave-packet superposition with $p_{01} = 10$ and $p_{02} = -30$. The value of the other relevant parameters are $\sigma_{01} = \sigma_{02} = 0.5$ and $\alpha = 1$. (*b*) Quantum trajectories associated with the dynamics described by the situation displayed in panel (*a*).

Moreover, as before, the initial distance between both wave packets is such that the initial overlapping is negligible.

Case A is represented in figure 4, where we can observe that varying the moduli of the initial average momenta only produces an asymmetric shift of the final positions of the wave packets with respect to $x = 0$ (see panel (*a*)), which is a result of the distortion of the boundary between regions I and II (the final wave packets are not symmetrically distributed with respect to $x = 0$). This boundary evolves in time at the same constant velocity than the corresponding expected value of the velocity for the total superposition,

$$\bar{v}_{\mathrm{A}} = \frac{\bar{p}_{\mathrm{A}}}{m} = \frac{\langle \Psi_{\mathrm{A}}^{*} | \hat{p} | \Psi_{\mathrm{A}} \rangle}{m} = \frac{p_{01} + p_{02}}{2m}, \tag{33}$$

because both wave packets are identical and normalized (see equation (16)). In particular, since $p_{01} = 10$ and $p_{02} = -30$, we have $\bar{v}_{\mathrm{A}} = -10$. Integrating the equation of motion $\dot{\bar{x}}_{\mathrm{A}} = \bar{v}_{\mathrm{A}}$ (according to Ehrenfest's theorem [27]), we obtain

$$\bar{x}_{\mathrm{A}}(t) = \bar{x}_0 + \bar{v}_{\mathrm{A}} t, \tag{34}$$

with $\bar{x}_0 = \langle \Psi^{*} | \hat{x} | \Psi \rangle = (x_{01} + x_{02})/2$. Equation (34) describes the time evolution of the boundary between regions I and II in this case—note that for $p_{02} = -p_{01}$, we recover again the time-independent boundary found for identical wave packets, studied in the previous section. As expected, this boundary also defines the non-crossing line for the associate quantum trajectories, which forbids the trajectory transfer from one region to the other one and vice versa, as seen in figure 4(*b*). Because of this property, we find that the two wave packets behave like two classical particles undergoing an elastic scattering: there is only transfer (indeed, exchange) of momentum during the scattering process, but the net balance of probability is zero since no trajectories are transferred. Moreover, note that indeed this effect will not be noticeable unless one looks at the quantum trajectories—as seen in panel (*a*), the evolution of the wave packets does not provide any clue on it.

In case B, since both velocities are equal in modulus, after interference the centers of the outgoing wave packets occupy symmetric positions with respect to $x = 0$, as seen in figure 5(*a*) (only the different width disturbs the full symmetry). However, as in case A, the

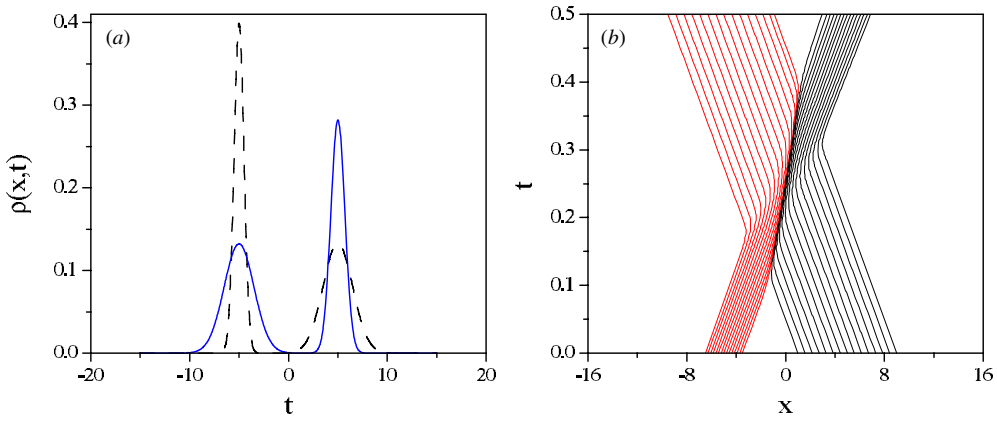

Figure 5. (*a*) Probability density at $t = 0$ (black dashed line) and $t = 0.8$ (blue solid line) for a wave packet superposition with $\sigma_{01} = 0.5$ and $\sigma_{02} = 1.5$. The value of the other relevant parameters are $|p_{01}| = |p_{02}| = 20$ and $\alpha = 1$. (*b*) Quantum trajectories associated with the dynamics described by the situation displayed in panel (*a*).

lack of total symmetry also causes the distortion of the boundary between regions I and II (see panel (*b*)), with a similar behavior regarding the non-crossing (or non-transfer) property. Now, since the modulus of both momenta are the same, $\langle\Psi^*|\hat{p}|\Psi\rangle = 0$ and therefore we cannot appeal to the same argument as before to explain this distortion effect. However, there is still a sort of effective 'internal' momentum which depends on the ratio between the widths of the wave packets. Assuming that the spreading is basically constant for the time we have propagated the trajectories, the corresponding effective velocity is given by

$$\bar{v}_{\mathrm{B}} = \frac{\sigma_{01}^{-1} v_{01} + \sigma_{02}^{-1} v_{02}}{\sigma_{01}^{-1} + \sigma_{02}^{-1}} = \left(\frac{\sigma_{02} - \sigma_{01}}{\sigma_{01} + \sigma_{02}}\right) v_0, \tag{35}$$

with $v_{01} = v_0 = -v_{02}$ ($v_0 > 0$); since the width of the wave packets varies in time, a slight time dependence can be expected in $\bar{v}_{\mathrm{B}}$, although in our case, as can be noted from figure 5(*b*), it can be neglected for practical purposes. Substituting the numerical values used in the propagation into (35), we find $\bar{v}_{\mathrm{B}} = 5$. The boundary or non-crossing line will be then given by

$$\bar{x}_{\mathrm{B}}(t) = \bar{x}_0 + \bar{v}_{\mathrm{B}} t, \tag{36}$$

where

$$\bar{x}_0 = \frac{\sigma_{01}^{-1} x_{01} + \sigma_{02}^{-1} x_{02}}{\sigma_{01}^{-1} + \sigma_{02}^{-1}} = -\left(\frac{\sigma_{02} - \sigma_{01}}{\sigma_{01} + \sigma_{02}}\right) x_0, \tag{37}$$

with $x_{02} = -x_{01} = x_0$ ($x_0 > 0$)—note that, otherwise, $\bar{x}_0 = 0$, as infers from figure 5(*a*), since the larger width of one of the wave packets balances the effect of the larger height of the other one. Despite this internal redistribution or balance of momentum, it is clear that we find again, as in case A, an elastic collision-like behavior.

The effect of an effective internal momentum could be explained by considering that, in this case, the relative size of the wave packets acts like a sort of *quantum inertia* or effective mass. Consider the trajectories associated with the wave packet with smaller value of σ_0 (black trajectories in figure 5(*b*)). As can be noted, it takes approximately 0.2 time units the whole swarm to leave the scattering or collision region (along the non-crossing boundary)—or,

equivalently, to revert the sign of the momentum of all the trajectories constituting the swarm and get their final asymptotic momenta. On the other hand, the trajectories associated with the wave packet with larger σ_0 (red trajectories in figure 5(b)) revert their momenta much faster, in about 0.1 time units—of course, we are not considering here the time that trajectories keep moving along the boundary, since the total 'interaction' time has to be the same for both swarms of trajectories. Thus, we find that the larger the spreading momentum, the larger the quantum inertia of the swarm of particles to change the propagation momentum and, therefore, to reach the final state.

We would also like to note another interesting property associated with case B. Consider that both wave packets lack their corresponding normalizing factor A_t when introduced in the superposition. If we then compute the expected value of the momentum, for instance, we obtain

$$\langle \hat{p} \rangle_{\mathrm{B}} = \frac{\langle \Psi_{\mathrm{B}}^{*} | \hat{p} | \Psi_{\mathrm{B}} \rangle}{\langle \Psi_{\mathrm{B}}^{*} | \Psi_{\mathrm{B}} \rangle} = \frac{\sigma_{01} v_{01} + \sigma_{02} v_{02}}{\sigma_{01} + \sigma_{02}} = \left(\frac{\sigma_{01} - \sigma_{02}}{\sigma_{01} + \sigma_{02}} \right) p_0, \tag{38}$$

i.e., there should be a certain 'drift' toward region I, such as in case A—and the same holds if we compute instead the expected value of the position. Note that in the previous case the normalization of each Gaussian wave packet produces a balance: the probability with which each wave packet contributes to the superposition is the same $\left(c_1^2 = c_2^2 = 1/2\right)$ because the width of one compensates the height of the other, as explained above. Therefore, the expected value of both position and momentum have to be zero. However, this compensation does not happen now: both wave packets have the same height although their widths differ, thus contributing with different probabilities P to the superposition,

$$P_1 = \frac{\sigma_{01}}{\sigma_{01} + \sigma_{02}} \qquad \text{and} \qquad P_2 = \frac{\sigma_{02}}{\sigma_{01} + \sigma_{02}}, \tag{39}$$

which produce the results observed in figure 6 (again, we assume that $\sigma_t \approx \sigma_0$ for the time considered). However, by inspecting (38), we note that if we add the averaged momentum $\bar{p}_{\mathrm{B}} = m\bar{v}_{\mathrm{B}}$, the total average momentum vanishes. Somehow the averaging defined by (38) acts as in classical mechanics, when a certain magnitude (e.g., the position or the momentum) is computed with respect to the center of mass of a system. Here, $\bar{p}_{\mathrm{B}}$ is the magnitude necessary to reset the superposition of non-normalized Gaussian wave packets to a certain 'center of spreading'. On the other hand, it is also important to stress the fact that, in this case, the clear boundary between the swarms of trajectories associated with each initial wave packet disappears. Now, although there is still a boundary, it does not prevent for the transfer of trajectories from one region to the other, as before. This effect, similar to consider inelastic scattering in classical mechanics, arises as a consequence of having wave packets with different probabilities, which we analyze below.

As seen above, unless there is an asymmetry in the probabilities carried by each partial wave in the superposition, there is always a well-defined boundary or non-crossing line between regions I and II. However, in the second example of case B, we have observed that it is enough an asymmetry in the probability distribution to break immediately the non-crossing line. Instead of using non-normalized Gaussian wave packets, let us consider case C, which is equivalent although the asymmetry is caused by $\alpha \neq 1$ instead of the wave-packet normalization. As we have seen in the two previous cases, provided both wave packets have the same weight (or, at least, both contribute equally to the superposition), the corresponding quantum trajectories, even if they are evenly distributed (equidistant) along a certain distance initially, they are going to give a good account of the whole dynamics. However, if the weights change, the same does not hold anymore. Somehow equal weights (or equal probabilities) mean the division of the coordinate space into two identical regions, each one influenced only

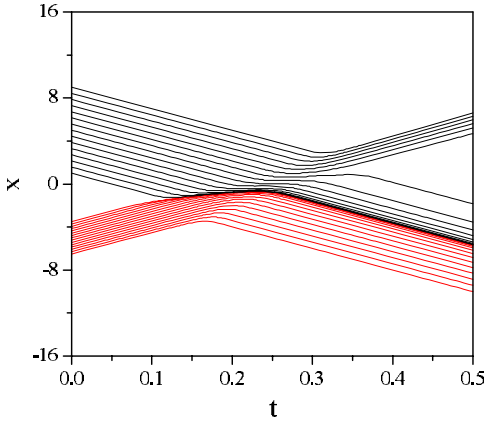

Figure 6. Bohmian trajectories associated with a Gaussian wave-packet superposition with $\sigma_{01} = 0.5$ and $\sigma_{02} = 1.5$. The value of the other relevant parameters are $p_{01} = -p_{02} = 20$ and $\alpha = 1$.

by the corresponding wave packet. In other words, there are always two well-defined swarms of trajectories, each one associated with one of the initial wave packets. When the weights change, apparently we have something similar to what we have been observing until now: the wave packets exchange their positions (see figure 7(*a*)). However, when we look at the associate quantum trajectories, we realize that there is transfer or flow of trajectories from one of the initial swarms to the other one. This transfer takes place from the swarm with larger weight to the lesser one, thus distorting importantly the boundary between regions I and II, as seen in figure 7(*b*), where this boundary lies somewhere between the two trajectories represented in blue (the trajectories that are closer to $x = 0$ in each swarm). However, note that this does not imply that the number of trajectories varies in each region asymptotically, but only the number of them belonging to one or the other wave packet. Thus, if initially we have $N_1 \propto c_1^2$ trajectories associated with ψ_1 and $N_2 \propto c_2^2$ with ψ_2, asymptotically we will observe $N_1' = (1-\alpha)N_1 \propto c_2^2$ and $N_2' = N_2 + \alpha N_1 \propto c_1^2$ due to the trajectory transfer. Unlike the two previous cases discussed above, this process can then be compared with inelastic scattering, where, after collision, not only the probability fluxes but also the number of particles changes. Accordingly, it is also important to mention that, due to the trajectory transfer, representations with evenly distributed trajectories are not going to provide a good picture of the problem dynamics, as infered from figure 6. Rather, we can proceed in two different ways. The obvious procedure is to consider initial positions distributed according to the corresponding (initial) probability densities. This procedure carries a difficulty: the number of trajectories needed to have a good representation of the dynamics may increase enormously depending on the relative weights. The second procedure is to consider evenly spaced values of the probability density and allocate at such space points the initial positions of the trajectories, as we have done to construct figure 7(*b*). In this case, although the trajectories will not accumulate exactly along the regions with larger values of the probability density, this construction has the advantage that we can follow the transport of equi-spaced probabilities along each particular trajectory. To make more apparent the difference in the relative number of trajectories (probability density) associated with each initial wave packets, we have considered $N_1 = 23$ and $N_2 = 11$ (i.e., $N_2/N_1 \sim 0.48 \approx c_2^2/c_1^2 = 0.5$). After scattering, the numbers that we have are $N_1' = 11$ and $N_2' = 23$, which are in the expected ratio $c'^2_2/c'^2_1 = c_1^2/c_2^2 = 2$.

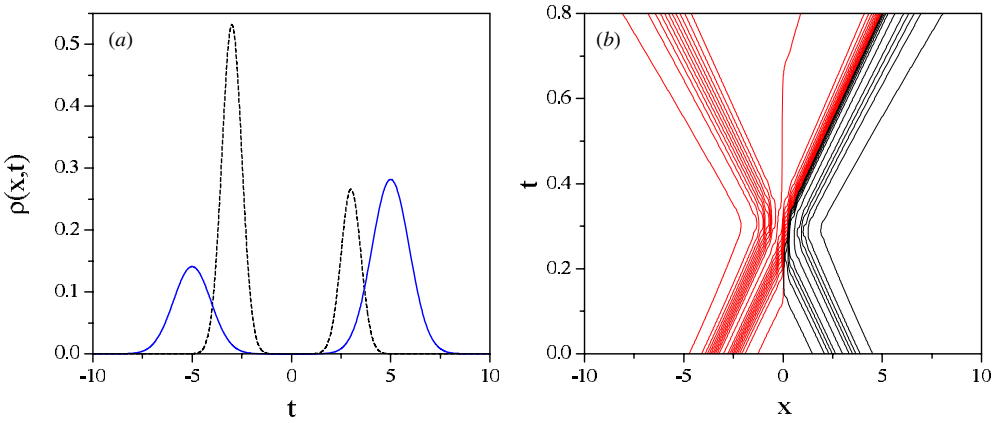

Figure 7. (*a*) Probability density at $t = 0$ (black dashed line) and $t = 0.8$ (red solid line) for a wave packet superposition with $\alpha = 0.5$ (i.e., $c_1^2 = 2/3$ and $c_2^2 = 1/3$). The value of the other relevant parameters are $p_{01} = -p_{02} = 10$ and $\sigma_{01} = \sigma_{02} = 0.5$. (*b*) Quantum trajectories associated with the dynamics described by the situation displayed in panel (*a*). The initial conditions for the quantum trajectories have been assigned by considering the different weights associated with each wave packet.

As said at the beginning of this subsection, here we have only considered the collision-like case. The same kind of results are expected for the analogous diffraction-like cases, with the addition that they manifest as a loss of fringe visibility. Thus, for cases A and B, one could appreciate a well-defined non-crossing line and a loss of fringe visibility due to the divergent velocities, v_p and v_s, respectively. And, for case C (or the second example in case B), the loss of fringe visibility would be caused by the transfer of trajectories, which would also lead to the distortion of the non-crossing line.

3.4. Coherent superpositions, potential barriers and resonances

Finally, here we are going to analyze an interesting effect associated with the non-crossing property described in the previous sections. Consider a Gaussian wave packet scattered off an impenetrable potential wall (for simplicity, we will assume $v_p > v_s$ for now). After some time the wave packet will collide with the wall and then part of it will bounce backward. The interference of the forward (f) and backward (b) wave packets will lead to a fringe-like pattern similar to those observed in the previous sections (see red solid line in figure 8(*a*)), with also a time, $t_{\max}^{\text{int}}$, for which the interference fringes are maximally resolved. Putting aside the initial Gaussian shape of the wave packet (and, therefore, the effects associated with v_s), if this process is represented as

$$\Psi = \psi_f + \psi_b \sim \mathrm{e}^{\mathrm{i}mv_px/\hbar} + \mathrm{e}^{-\mathrm{i}mv_px/\hbar} \tag{40}$$

at $t_{\max}^{\text{int}}$, we obtain $\rho(x) \sim \cos^2(mv_px/\hbar)$. The distance between two consecutive minima is then $w_0 = \pi\hbar/mv_p$, which turns out to be the same distance between two consecutive minima in the two wave-packet interference process (see black dashed line in figure 8(*a*)). That is, although each process has a different physical origin (barrier scattering versus wave packet collision), the effect is similar—there is a certain shift in the position of the corresponding maxima ($\sim\pi/2$), which arises from the fact that, in the case of barrier scattering, the impenetrable wall forces the wavefunction to have a node at $x = 0$. If now we go to the

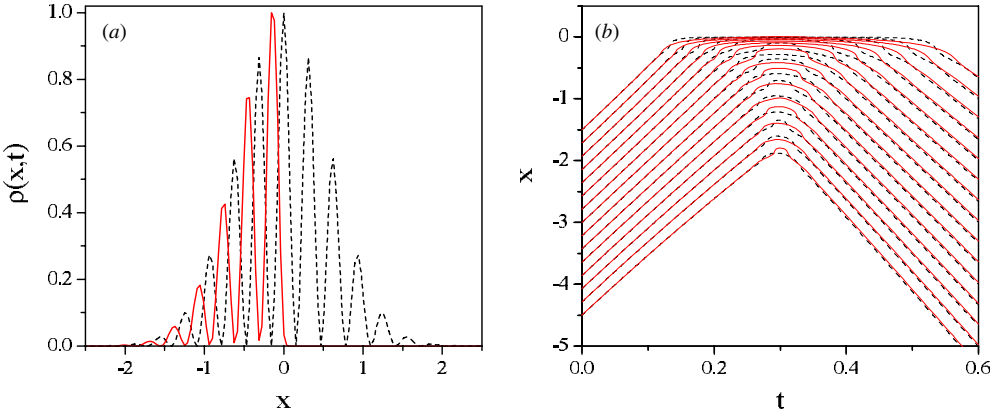

Figure 8. (*a*) Probability density at $t = 0.3$ for the collision of a Gaussian wave packet off: an external impenetrable wall (red solid line) and another (identical) Gaussian wave packet (black dashed line). To compare, the maxima of both probability densities are normalized to unity. (*b*) Bohmian trajectories illustrating the dynamics associated with the two cases displayed in part (*a*). Here, $v_p = 10$ and $v_s = 1$.

corresponding quantum trajectories, we observe (see figure 8(*b*), with red solid line) that as the wave packet starts to 'feel' the presence of the wall, the trajectories bend gradually (in the x versus t representation) and then start to move in the opposite direction. When these trajectories are compared with those associated with the problem of the two wave-packet superposition, the resemblance between trajectories with the same initial positions is excellent, except in the interference region due to the different location of the nodes of the corresponding wavefunctions—these differences are the trajectory counterpart of the shift mentioned before.

From the previous description one might infer that, since the dynamics for $x < 0$ and for $x > 0$ do not mix (due to non-crossing), each half of the central interference maximum arises from different groups of trajectories. Thus, in principle, one should be able to arrange the impenetrable wall problem in such a way that allows us to explain this effect. Within this context, although all the peaks have the same width as in the wave-packet superposition problem, the closest one to the wall should have half such a width, i.e., $w \sim \pi\hbar/2p = w_0/2$. Due to boundary conditions and the forward–backward interference discussed above, it is clear that this peak cannot arise from interference, but from another mechanism: a *resonance* process. Therefore, apart from the wall, we also need to consider the presence of a potential well. In order to observe a resonance or quasi-bound state, the width of this well should be, at least, of the order of the width w of the bound state. From standard quantum mechanics, we know that in problems related to bound states in finite-well potentials the relationship [27]

$$V_0 a^2 = n\frac{\hbar^2}{2m} \tag{41}$$

always appears, where a is the half-width of the well ($a = w/2$) and n is an integer number. The eventual solutions (bound states) are then observable or not depending on whether the condition to which it might correspond will be in consonance or not with this condition. In our case, we can use (41) to obtain an estimate of the well depth, which results

$$V_0 = \frac{16}{\pi^2}\frac{p^2}{2m} \tag{42}$$

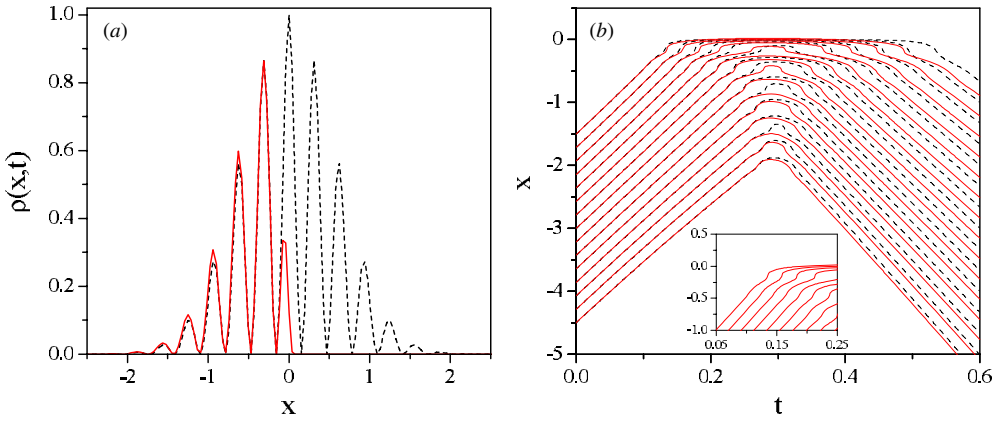

Figure 9. (*a*) Probability density at $t = 0.3$ for the collision of a Gaussian wave packet off: the external potential described by equation (43) (red solid line) and another (identical) Gaussian wave packet (black dashed line). To compare, the maxima at $x \approx -0.32$ of both probability densities are normalized to the same height (the maximum at $x = 0$ of the two wave packet probability density being set to unity). (*b*) Bohmian trajectories illustrating the dynamics associated with the two cases displayed in part (*a*). Inset: enlargement of the plot around $t = 0.15$ to show the action of the potential well on the trajectories started closer to $x = 0$. Here, $v_p = 10$ and $v_s = 1$.

when we assume $n = 1$. Now, we then have a potential which presents a short-range attractive well before reaching the impenetrable wall,

$$V(x) = \begin{cases} 0 & x < -w \\ -V_0 & -w \leqslant x \leqslant 0 \\ \infty & 0 < x. \end{cases} \tag{43}$$

If we compute now $\rho(\mathbf{r}, t)$ at $t_{\max}^{\text{int}}$, we obtain the result displayed in figure 9(*a*). As can be noted, now there is an excellent matching of the peak widths, with the closest one to the wall being half-width when compared with the remaining ones—the associate quantum trajectories are displayed and compared in figure 9(*b*).

The equivalence between the two wave-packet collisions and the scattering of a wave packet off a potential is not restricted to the condition $v_p > v_s$, but it is of general validity. As shown in figure 5, it also holds for the diffraction-like situation, i.e., $v_p < v_s$. In figure 10(*a*), we show that half of the diffraction-like pattern is again well reproduced after replacing one of the wave packets by an external potential, and the same also happens for the corresponding quantum trajectories (see figure 10(*b*)). However, in order to find these results, now a subtlety has to be considered: the central diffraction maximum increases its width with time. In terms of simulating this effect with a potential function, it is clear that the width of the potential well should also increase with time. Thus, we need to consider a 'dynamical' or time-dependent potential function rather than a static one, as done before. In order to determine this potential function, we proceed as before. First, we note that the two wave-packet collision problem, equation (24), is explicitly written in terms of Gaussian wave packets (see equation (16)) as

$$\Psi \sim \mathrm{e}^{-(x+x_t)^2/4\tilde{\sigma}_t\sigma_0 + \mathrm{i}p(x+x_t)/\hbar + \mathrm{i}Et/\hbar} + \mathrm{e}^{-(x-x_t)^2/4\tilde{\sigma}_t\sigma_0 - \mathrm{i}p(x-x_t)/\hbar + \mathrm{i}Et/\hbar}, \tag{44}$$

where

$$x_t = x_0 - v_p t \tag{45}$$

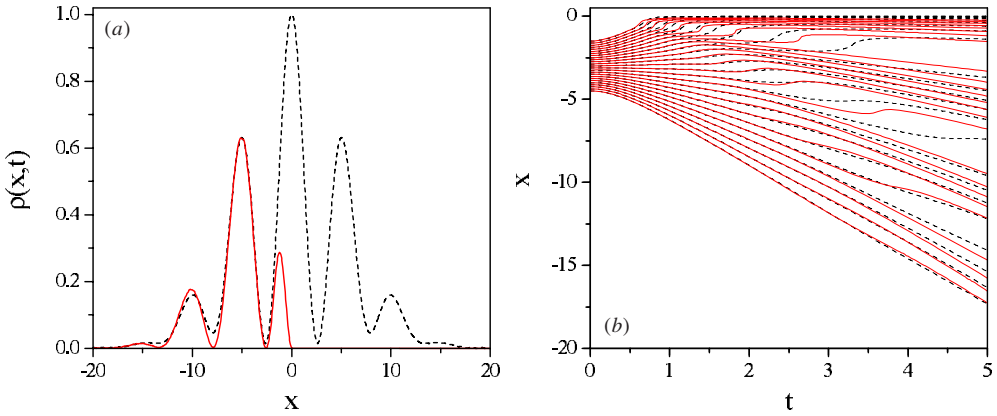

Figure 10. (*a*) Probability density at $t = 5$ for the collision of a Gaussian wave packet off: the external, time-dependent potential described by equation (53) (red solid line) and another (identical) Gaussian wave packet (black dashed line). To compare, the maxima at $x \approx -5$ of both probability densities are normalized to the same height (the maximum at $x = 0$ of the two wave packet probability density being set to unity). (*b*) Bohmian trajectories illustrating the dynamics associated with the two cases displayed in part (*a*). Here, $v_p = 0.1$ and $v_s = 1$.

(for simplicity, we have neglected the time-dependent prefactor, since it is not going to play any important role regarding either the probability density or the quantum trajectories). The probability density associated with (44) is

$$\rho(x,t) \sim \mathrm{e}^{-(x+x_t^2)/2\sigma_t^2} + \mathrm{e}^{-(x-x_t^2)/2\sigma_t^2} + 2\mathrm{e}^{-(x^2+x_t^2)/2\sigma_t^2} \cos\left[f(t)x\right], \tag{46}$$

with

$$f(t) \equiv \frac{\hbar t}{2m\sigma_0^2}\frac{x_t}{\sigma_t^2} + \frac{2p}{\hbar}. \tag{47}$$

As can be noted, (46) is maximum when the cosine is +1 (constructive interference) and minimum when it is −1 (destructive interference). The first minimum (with respect to $x = 0$) is then reached when $f(t)x = \pi$, i.e.,

$$x_{\min}(t) = \frac{\pi}{\frac{2p}{\hbar} + \frac{\hbar t}{2m\sigma_0^2}\frac{x_t}{\sigma_t^2}} = \frac{\pi\sigma_t^2}{\frac{2p\sigma_0^2}{\hbar} + \frac{\hbar t}{2m\sigma_0^2}x_0}, \tag{48}$$

for which

$$\rho[x_{\min}(t)] \sim 4\mathrm{e}^{-(x_{\min}^2+x_t^2)/2\sigma_t^2} \sinh\left(\frac{x_{\min}x_t}{2\sigma_t^2}\right), \tag{49}$$

which is basically zero if the initial distance between the two wave packets is relatively large when compared with their spreading.

In figure 11(*a*), we can see the function $x_{\min}(t)$ for different values of the propagation velocity v_p. As seen, $x_{\min}(t)$ decreases with time up to a certain value, and then increases again, reaching a linear asymptotic behavior. From (48) we find that the minimum value of $x_{\min}(t)$ is reached at

$$t_{\min} = \frac{4m\sigma_0^4}{\hbar^2 x_0}\left[-p + \sqrt{p^2 + p_s^2\left(\frac{x_0}{\sigma_0}\right)^2}\right]. \tag{50}$$

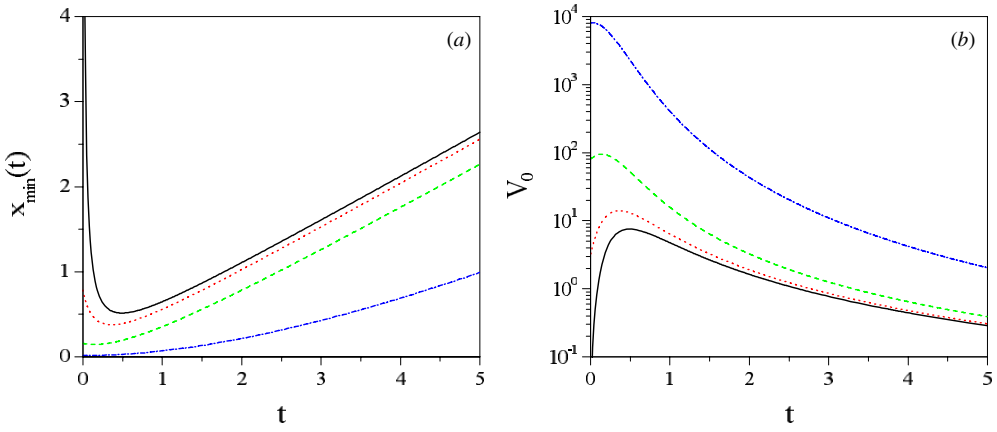

Figure 11. (*a*) Plot of $x_{\min}$ as a function of time for different values of the propagation velocity: $v_p = 0.1$ (black solid line), $v_p = 2$ (red dotted line), $v_p = 10$ (green-dashed line) and $v_p = 100$ (blued dash-dotted line). (*b*) Plot of V_0 as a function of time for the same four values of v_p considered in panel (*a*). In all cases, $v_s = 1$.

The linear time dependence at long times is characteristic of the Fraunhofer regime, where the width of the interference peaks increases linearly with time. On the other hand, the fact that, at $t = 0$, $x_{\min}(t)$ increases as v_p decreases (with respect to v_s) could be understood as a 'measure' of the coherence between the two wave packets, i.e., how important the interference among them is when they are far apart (remember that, despite their initial distance, there is always an oscillating term in between due to their coherence [28]). Note that this is in accordance with the standard quantum-mechanical arguments that interference-like patterns are manifestations of the wavy nature of particles, while scattering-like ones display their corpuscle nature (more classical like). Thus, as the particle becomes more 'quantum mechanically', the initial reaching of the 'effective' potential well should be larger. And, as the particle behaves in a more classical fashion, this reaching should decrease and be only relevant near the scattering or interaction region, around $x = 0$. From equation (48), two limits are thus worth discussing. In the limit $p \sim 0$,

$$x_{\min}(t) \approx \frac{\pi \sigma_t^2}{x_0} \frac{\tau}{t} \tag{51}$$

and $t_{\min} \approx \tau$. In the long-time limit, this expression becomes $x_{\min}(t) \approx (\pi\hbar/2m)(t/x_0)$, i.e., $x_{\min}$ increases linearly with time, as mentioned above. On the other hand, in the limit of large σ_0 (or, equivalently, $v_p \gg v_s$),

$$x_{\min}(t) \approx \frac{\pi\hbar}{2p} \tag{52}$$

and $t_{\min} \approx 0$. That is, the width of the 'effective' potential barrier remains constant in time, this justifying our former hypothesis above, in the scattering-like process, when we considered $w \sim \pi\hbar/2p$.

After equation (48), the time-dependent 'effective' potential barrier is defined as (43),

$$V(t) = \begin{cases} 0 & x < x_{\min}(t) \\ -V_0[x_{\min}(t)] & x_{\min}(t) \leqslant x \leqslant 0 \\ \infty & 0 < x. \end{cases} \tag{53}$$

with the (time-dependent) well depth being

$$V_0[x_{\min}(t)] = \frac{2\hbar^2}{m}\frac{1}{x_{\min}^2(t)}. \tag{54}$$

The variation of the well depth along time is plotted in figure 11(*a*) for the different values of v_p considered in figure 11(*b*). As seen, the well depth increases with v_p (in the same way that its width, $x_{\min}$, decreases with it) and decreases with time. For low values of v_p, there is a maximum, which indicates the formation of the quasi-bound state that will give rise to the innermost interference peak (with half the width of the remaining peaks, as shown in figure 10(*a*)). Note that, despite the time dependence of the well depth, in the limit $v_p \gg v_s$, we recover equation (42).

We have shown that the problem of the interference of two colliding wave packets can be substituted by the problem of the collision of a wave packet off a potential barrier. Although the model that we have presented is very simple, it is important to stress that it reproduces fairly well the dynamics involved—of course, one can always search for more refined and precise models. The fact that one can make this kind of substitution puts quantum mechanics and the superposition principle on the same grounds as two important frameworks in classical physics (one could think of many other situations, but these two ones are particularly general and well known). The first one is widely used in classical mechanics (and then, in its quantized version, also in quantum mechanics): it is the equivalence between a two-body problem and a one-body problem acted by a central force. As can be noted, our reduction is of the same kind: a two wave-packet dynamical process can be reduced to the dynamics of a single wave packet subjected to the action of an external potential. The second framework is the one provided by the so-called method of images, widely used in electrostatics: the interaction between a charge distribution and a conductor can be replaced by the interaction between such a charge distribution and another virtual one. This would be the reciprocal situation to ours: the dynamics induced by an external potential on a wave packet can be translated as the dynamics taking place when two wave packets (ours and a virtual one) are considered.

4. Final discussion and conclusions

Here we have presented a detailed analysis of quantum interference within the framework of quantum trajectories. As we have shown, there are at least two important properties which are masked when interference is studied from the standard point of view, but that become apparent as soon as we move to the Bohmian domain: (*a*) it is always possible to determine uniquely the departure region of a particle from the final outcome and (*b*) interference can be described as an effect similar to that of particle–particle collisions. Bohmian trajectories allow one to determine the origin of the particles that contribute to each final wave packet, contrary to the standard view of interference processes, where the final wave packets are commonly associated with the time-evolved initial ones, according to the superposition principle. Nevertheless, as has also been shown here, putting aside the superposition principle and considering the properties of the quantum current density, it is also possible to reach similar conclusions in standard quantum mechanics (although, to our knowledge, one cannot find this in the literature). Of course, although we might know that quantum particles are associated with one wave packet or the other during the whole propagation, this should not be mistakenly considered as to have a complete knowledge of the their corresponding initial positions in the experiment,—remember that the initial positions distribute in a *random* fashion following the initial probability density.

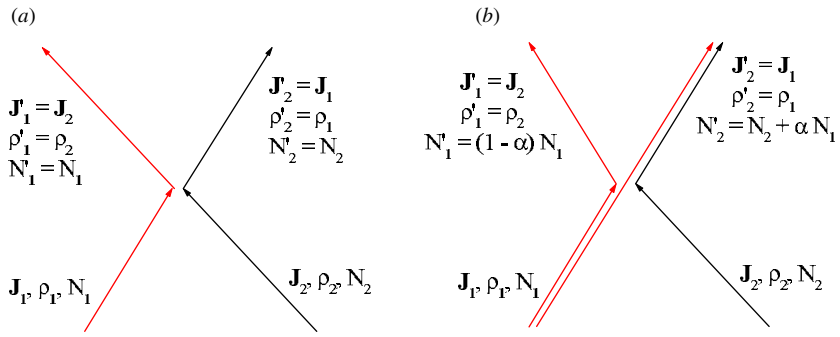

Figure 12. Schematic representation of the two types of processes that may take place in two wave-packet collisions: (*a*) elastic-like scattering and (*b*) inelastic-like scattering. See the text for details.

To some extent, the property (*a*) can then be regarded as a sort of distinguishability, which should not be confused with that one arising when one considers the problem of identical (fermion or boson) particles. Rather, this issue is connected with the property (*b*) in the sense that it allows us to describe the process, in the collision-like case, as classical collisions. Two situations can then happen. If the probability is equi-distributed between the two wave packets, the effect is similar to classical elastic particle–particle collisions, where only the momentum is transferred. In our case, what is transferred is the probability distribution through the probability density current, since the number of particles associated with each wave packet remains the same. This situation, represented schematically in figure 12(*a*), corresponds to the cases A and the first one of B described in section 3.3. On the other hand, when the probabilities are asymmetrically distributed, there is a probability transfer which translates into a trajectory transfer—the well-defined non-crossing line then disappears. This behavior, which is similar to a classical inelastic particle–particle collision, is displayed in figure 12(*b*) and corresponds to the case C and the second example of B (see section 3.3). Rather than being just a conceptual discussion, it is worth noting that this analysis can be of much applied importance in the design, development, improvement and/or implementation of new trajectory-based algorithms [21], where one of the main problems is precisely the way to deal with separate (in space) wave packets and the nodes emerging from their interference.

As has been noted, observing collision-like behaviors or not depends on the relation between the spreading and the propagation velocities of the wave packets. If v_p is larger than v_s, one will observe collision-like behaviors, which, to some extent, is the same to say that the wave packets behave like classical particles or *corpuscles*. Of course, note that when we use the concept 'collision' we are not referring exactly to a true particle–particle collision, since the two wave packets indeed refer to the *same* system (which, by means of any of the procedures mentioned in section 1, for instance, has been split up and converted into a so-called Schrödinger cat system). On the other hand, when v_s dominates the dynamics, the behavior is diffraction like. The wave packets then behave in a wavy manner and diffraction patterns appear after their interference.

Finally, it is also very important the fact that wave-packet interference problems can be understood within the context of scattering off effective potential barriers. As is well known, in classical mechanics one can substitute a particle–particle scattering problem by that of an effective particle (associated with the center of the mass of the particle–particle system) acted by an (also effective) interaction central potential. Similarly, here we have shown that any

interference process (either collision-like or diffraction-like) can also be rearranged in such a way that the two wave-packet problem can be replaced by that of a (single) wave-packet scattering off an effective (time-dependent) potential barrier. In this regard, we would like to note that this property could be considered a precursor of more refined and well-known methods used to deal with many body systems, where the many degrees of freedom are replaced by a sort of effective time-dependent potential [29]. Furthermore, it is worth stressing that, in order to describe properly the interference fringes during the process, we have shown that these potentials have to support temporary bound states or resonances. In those cases where the non-crossing boundary disappears because the probability is not equally distributed between the two wave packets, the impenetrable barriers should be replaced by 'transparent' or step barriers. Thus, in the same way that after the collision process part of the trajectories associated with one of the wave packets become attached to the other wave packet, after the collision with the transparent barrier part of the trajectories will move on the barrier.

Acknowledgments

This work has been supported by the Ministerio de Ciencia e Innovación (Spain) under project no FIS2007-62006. A S Sanz also acknowledges the Consejo Superior de Investigaciones Científicas (Spain) for a JAE-Doc contract.

References

[1] Macchiavello C, Palma G M and Zeilinger A (eds) 1999 *Quantum Computation and Quantum Information Theory* (Singapore: World Scientific)
[2] Nielsen M A and Chuang I L 2000 *Quantum Computation and Quantum Information* (Cambridge: Cambridge University Press)
[3] Brumer P W and Shapiro M 2003 *Principles of the Quantum Control of Molecular Processes* (Hoboken, NJ: Wiley-Interscience)
[4] Schrödinger E 1935 *Proc. Cam. Phil. Soc.* **31** 555
Schrödinger E 1936 *Proc. Cam. Phil. Soc.* **32** 446
Einstein A, Podolsky B and Rosen N 1935 *Phys. Rev.* **47** 777
Bohm D 1951 *Quantum Mechanics* (New York: Dover)
[5] Feynman R P, Leighton R B and Sands M 1965 *Quantum Mechanics, The Feynman Lectures on Physics* vol 3 (Reading, MA: Addison-Wesley)
[6] Scalapino D J 1969 *Tunneling Phenomena in Solids* ed E Burstein and S Lundqvist (New York: Plenum) p 447
[7] Berman P R (ed) 1997 *Atom Interferometry* (San Diego: Academic)
[8] Shin Y, Saba M, Pasquini T A, Ketterle W, Pritchard D E and Leanhardt A E 2004 *Phys. Rev. Lett.* **92** 050405
[9] Zhang M, Zhang P, Chapman M S and You L 2006 *Phys. Rev. Lett.* **97** 070403
[10] Cederbaum L S, Streltsov A I, Band Y B and Alon O E 2007 *Phys. Rev. Lett.* **98** 110405
[11] Hänsel W, Reichel J, Hommelhoff P and Hänsch T W 2001 *Phys. Rev. Lett.* **86** 608
Hänsel W, Reichel J, Hommelhoff P and Hänsch T W 2001 *Phys. Rev.* A **64** 063607
[12] Hinds E A, Vale C J and Boshier M G 2001 *Phys. Rev. Lett.* **86** 1462
[13] Andersson E, Calarco T, Folman R, Andersson M, Hessmo B and Schmiedmayer J 2002 *Phys. Rev. Lett.* **88** 100401
[14] Kapale K T and Dowling J P 1995 *Phys. Rev. Lett.* **95** 173601
Thanvanthri S, Kapale K T and Dowling J P 2008 Arbitrary coherent superpositions of quantized vortices in Bose–Einstein condensates from orbital angular momentum beams of light arXiv:0803.2725v1
[15] Chapman M S, Ekstrom C R, Hammond T D, Schmiedmayer J, Tannian B E, Wehinger S and Pritchard D E 1995 *Phys. Rev.* A **51** R14
[16] Deng L, Hagley E W, Denschlag J, Simsarian J E, Edwards M, Clark C W, Helmerson K, Rolston S L and Phillips W D 1999 *Phys. Rev. Lett.* **83** 5407
[17] Bohm D 1952 *Phys. Rev.* **85** 166, 180
[18] Holland P R 1993 *The Quantum Theory of Motion* (Cambridge: Cambridge University Press)
[19] Sanz A S, Borondo F and Miret-Artés S 2002 *J. Phys.: Condens. Matter* **14** 6109

[20] Sanz A S and Miret-Artés S 2007 *J. Chem. Phys.* **126** 234106
[21] Wyatt R E 2005 *Quantum Dynamics with Trajectories* (New York: Springer)
[22] Born M 1926 *Z. Phys.* **37** 863
Born M 1926 *Z. Phys.* **38** 803
[23] Madelung E 1926 *Z. Phys.* **40** 332
[24] Berry M V and Balazs N L 1979 *Am. J. Phys.* **47** 264
Unnikrishnan K and Rau A R P *Am. J. Phys.* **64** 1034
Siviloglou G A, Broky J, Dogariu A and Christodoulides D N 2007 *Phys. Rev. Lett.* **99** 213901
[25] Sanz A S and Miret-Artés S 2007 *Chem. Phys. Lett.* **445** 350
[26] Sanz A S, Borondo F and Miret-Artés S 2000 *Phys. Rev.* B **61** 7743
[27] Schiff L I 1968 *Quantum Mechanics* 3rd edn (Singapore: McGraw-Hill)
[28] Sanz A S and Miret-Artés S 2008 *Chem. Phys. Lett.* **458** 239
[29] Sanz A S, Giménez X, Bofill J M and Miret-Artés S 2009 Time-dependent density functional theory from a Bohmian perspective *Chemical Reactivity Theory: A Density Functional View* ed P Chattaraj (New York: Francis and Taylor)